Jpn. J. Appl. Phys. Vol. 42 (2003) pp. 4067–4073
Part 1, No. 6B, June 2003

Development of Electrothermal Actuator with Optimized Motion Characteristics

Yen-Jyh LAI[1], Chengkuo LEE[1,*], Chia-Yu WU[1], Wen-Chih CHEN[1], Chihchung CHEN[1], Yu-Shen LIN[1], Weileun FANG[2] and Ruey-Shing HUANG[3]

[1]*Asia Pacific Microsystems, Inc., No. 2, R&D Road VI, Science-Based Industrial Park, Hsinchu, Taiwan*
[2]*Institute of MEMS, National Tsing Hua University, Hsinchu, Taiwan*
[3]*Institute of Electronics Eng., National Tsing Hua University, Hsinchu, Taiwan*

(Received November 13, 2002; accepted for publication January 22, 2003)

In this paper, we give the reasons for the phenomenon of adhesion of U-shaped electrothermal actuators onto substrates which is commonly observed for such devices. Next, we identified a significant advantage for operating these U-shaped actuators on top of a polysilicon layer with a suitable pattern design. A thorough investigation on the deflection behavior of actuators with different dimensional parameters, i.e., cold arm width, flexural beam length and hot arm length, was carried out. Finally, we discussed the effects of electrostatic force on the actuator due to these parameters. Based on these analyses, we suggested optimized dimensions for the U-shaped actuator. [DOI: 10.1143/JJAP.42.4067]

KEYWORDS: MEMS, electrothermal actuator, electrostatic force, stiction

1. Introduction

Microactuators for different actuation mechanisms, such as electrostatic, electromagnetic, piezoelectric and electrothermal devices have been demonstrated by means of micromachining technology. Among them, surface micromachined electrothermal actuators are very attractive for many applications, such as optical micro-electro-mechanical system (MEMS) and radio frequency (RF) MEMS, due to their advantages of relatively large output force and displacement. U-shaped electrothermal actuators with in-plane motion are the most well known ones.[1–3] Based on surface micromachining, the actuator consists of two arms of uneven widths suspended above the substrate with two anchor points. When power is applied from anchor to anchor, the arm with a larger electrical resistor and power generation will show higher temperature and larger volume expansion, i.e., the so-called hot arm. The other arm will be the cold arm. Since these two arms are connected at one end opposite to the anchors, the actuator will be forced to move in terms of an arc-like pattern due to the asymmetrical thermal expansion.

In the practical applications, the long-term motion stability of actuators is very crucial. Based on the experimental observation, however, we found that U-shaped electrothermal actuators often showed unstable motion. Since the electrothermal actuator is normally operated either under a constant voltage or current loading, an electrical space charge accumulated between the doped polycrystal Si actuator beam and doped Si substrate will occur. This motion instability is very possibly caused by floating-charge-induced electrostatic force. To the best knowledge of the authors, there is no related published literature available on this phenomenon and how it influences the motion stability. In this study, we investigate the motion behavior of a U-shaped actuator, and discuss the relations between the observed results and the influence of accumulated charge on the motion stability. Finally, we develop an electrothermal actuator and identify its optimum motion characteristics.

*Corresponding author. E-mail address: mems@apmsinc.com

2. Experimental Method

The devices presented in this paper were designed and fabricated using the multi-user MEMS processes (MUMPs).[4] The MUMPs service offers three layers of polysilicon and two sacrificial layers on a silicon nitride dielectric (SiN_x) layer covered substrate. Our U-shaped actuator beam was formed of the second polysilicon layer (POLY1 in MUMPs). This actuator might be either operated on a SiN_x layer covered substrate, i.e., type A, or on a POLY0/SiN covered substrate, i.e., type B, where the POLY0 layer is the first polysilicon layer in MUMPs. Actuators having the same dimensions as these two types were prepared for characterizations of motion behavior related to the accumulated electrical space charge. The layout diagram and related actuator scanning electron microscope (SEM) images are shown in Fig. 1. From Fig. 1 the major difference between types A and B is observed to be that the POLY0 is electrically connected to the actuator beam of POLY1 through the "bonding pad via" in the type B device. We also fabricated a type C device with an underlying POLY0 pattern that was electrically isolated from the actuator itself, as shown in Fig. 2. If we employ a probe or a bonding wire to electrically connect the underlying POLY0 pattern to one anchor of the actuator in the type C device, then the POLY0 of "plus" side is defined as type C1, and POLY0 of "negative" side is defined as type C2. Basically, type B devices are equivalent to type C2 actuators except that the Poly0 layer is connected to the cold arm pad directly and not through the probe or bonding wire. Additionally, we created some "dimples" in the cold arm for all types of devices in order to avoid surface-tension-induced adhesion during the wet etching release process.

In order to understand the origins of the electrothermal actuator motion instability, by comparing the data of types A, B, and C devices, we may identify the influences of attraction force due to the electrostatic force caused by the accumulated space charge, the friction force, and the electrostatic force attributed to a spatial capacitor between the parallel electrodes.

Using these devices, we characterized the electrostatic effect on actuators of various dimensions, when the unwanted attraction force could be removed after the origin

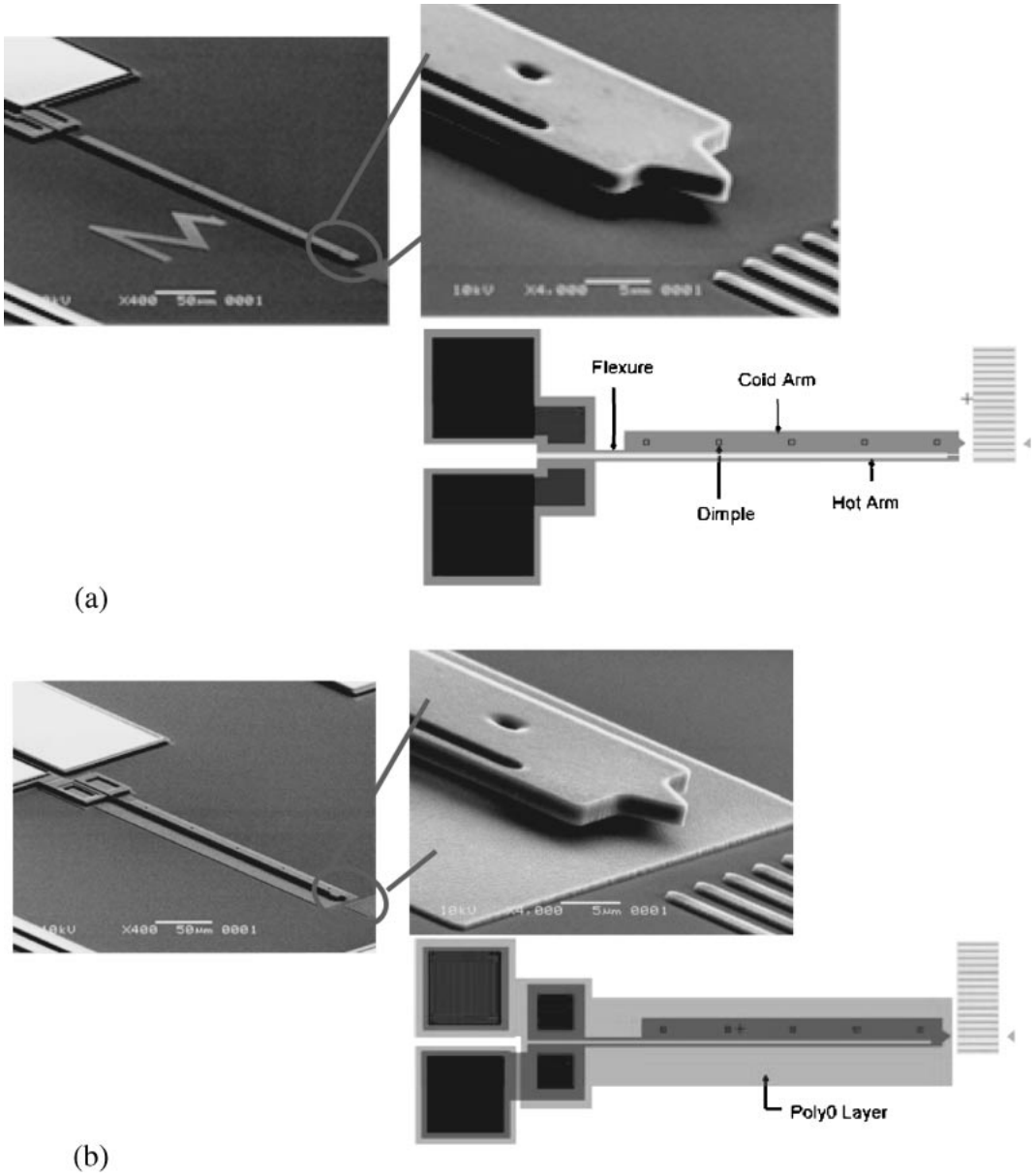

Fig. 1. Device layout drawing and related actuator SEM images (a) device was operated above the SiN_x layer (b) device was operated above the polysilicon layer.

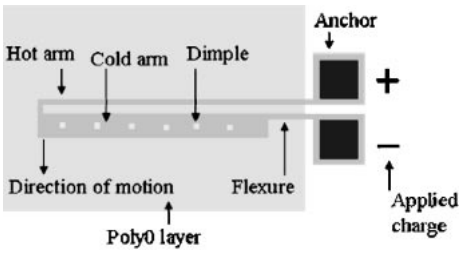

Fig. 2. Layout of type C device operated above an isolated polysilicon layer.

was discovered. On the other hand we also applied the finite element method (FEM) software, Ansys, in the present case, to understand the stiffness and output force of actuators with different geometries. Since the electrothermal actuation is a coupled-field problem (electrical, thermal and mechanical), it is difficult to find analytical solutions. These FEM analyses can help us understand the motion characteristics in terms of mechanical force and electrostatic force.

3. Results and Discussion

3.1 Origins of stiction and adhesion

The observation of dynamic motion behavior showed that, type A devices tended to snap down and adhere to the substrate during motion. Comparing the SEM images of Figs. 1 and 3, a smaller gap between the tip end of the actuator and substrate is observed in Fig. 3. We show a type A actuator adhered to the substrate, and the observed spacing is attributed to the dimple height. Moreover, for some type A devices, the motion speed was not very stable and the deflection decreased during the swing motion because of partial stiction.

Such motion instability might be possibly due to the friction force between the dimples of the cold arm and

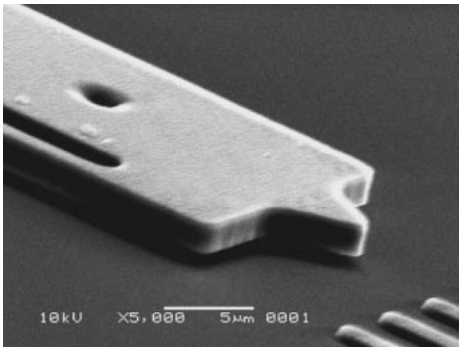

Fig. 3. SEM image for adhered type A device.

underlying materials. In fact, when we included the POLY0 layer underneath the POLY1 actuator beam, i.e., type B samples, the actuator motion became much more stable. According to the 3D interferometer measurements of the roughness of SiN_x, POLY0, and POLY1, their roughness values (rms value) were 1.97, 3.56, and 4.98 nm, respectively. This shows that the POLY0 layer is rougher than the SiN_x layer. The observed result, that the type B devices showed a more stable motion behavior than type A devices, has no contribution from the factor corresponding to roughness. Because the instability phenomenon of type A devices is somewhat random or suddenly occurred after different cycles of swing motion in numerous tests performed in the ambient-environment-controlled clean room, the origin of stiction during motion should have nothing to do with any factor related to moisture. After eliminating friction force and moisture from the possible origin of stiction, we may consider electrostatic force as a main factor. Again, since the geometric dimensions of A and B devices were the same, the mentioned electrostatic force could not be attributed to the spatial capacitor between the parallel electrodes. Instead, it could be a result of the floating charge accumulation.

Interestingly, if the Si substrate of type A samples was prepared with good electrical conduction to the Cu stage, as shown in Fig. 4, the instability phenomenon of type A devices disappeared. Figure 5 shows the measured displacement data versus the applied voltage for type A devices without/with the electrical space charge releasing treatment. Obviously, such a treatment allows type A devices to have larger displacement. We even determined that the adhered

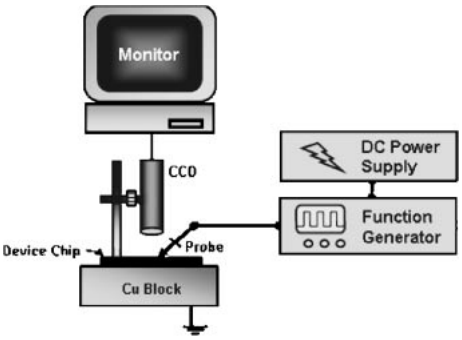

Fig. 4. Schematic testing system.

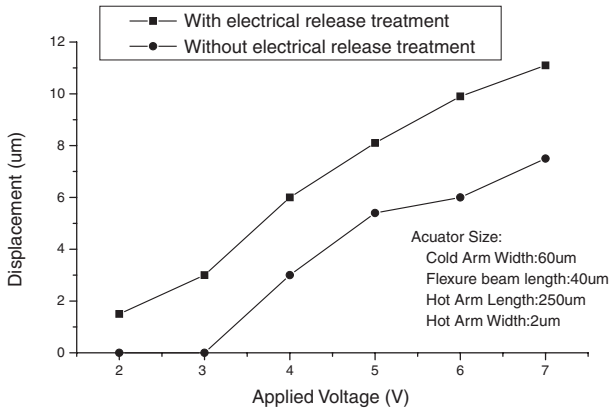

Fig. 5. Measured tip displacement for type A devices without/with electrical space charge releasing treatment.

actuator beam of type A samples would return to the normal position and showed good motion behavior again, after these devices were electrically grounded. It proves our viewpoint that floating charge accumulation is the main factor responsible for motion instability.

Although the stiction problem could be avoided with the help of the space charge releasing treatment, the setup seems a little inconvenient for practical applications. Compared with such a setup, the type B approach is much easier and more acceptable. Type B devices also show almost the same displacement performance as the type A devices with a good electrical grounding, as shown in Fig. 6.

In terms of preferring the POLY0 layer to realize motion stability, it appears that the semiconducting POLY0 layer could become a charge shielding layer to prevent the U-shaped actuator from the occurrence of unstable motion. In order to realize the actual mechanism, we may compare type B and type C devices. The POLY0 layer of type C device was electrically isolated from the POLY1 actuator beam itself. Based on the testing observation, however, the motion of type C devices was also influenced significantly by the accumulated space charge similar to that of type A devices. So, the assumption of shielding effect was wrong. Since the only difference between type B and type C devices is that, in type B, Ploy0 is connected to the "cold arm pad (anchor)",

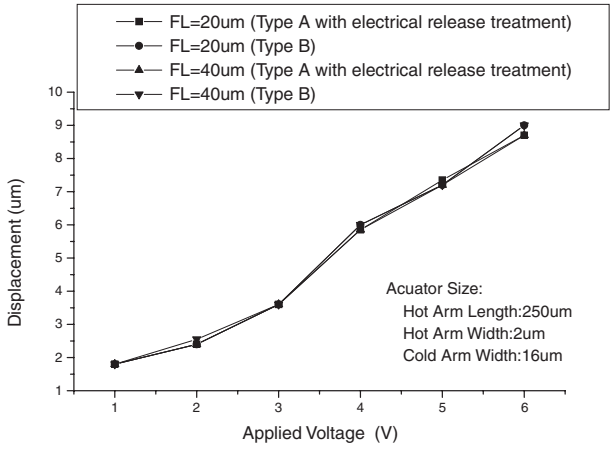

Fig. 6. Measured tip displacement for type A devices with electrical space charge releasing treatment and type B devices.

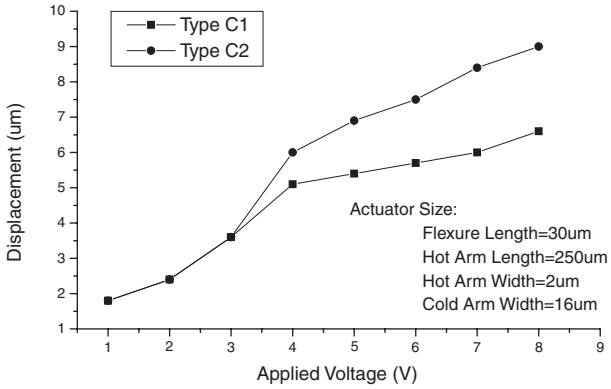

Fig. 7. Measured tip displacement for type C1 and C2 devices.

we compensated this difference by applying the same voltage to the Poly0 layer and the cold arm pad, i.e., similar to the type C2 configuration. Very interestingly, we found that the adhered actuator beam of type C devices reverted to a smooth motion behavior when a voltage was applied to type C devices to achieve type C2 configuration. This phenomenon was similar to that of the type A case by the electrical releasing treatment. As a result, we believed that type B design could also provide the actuator with a good charge release channel via the pad. This mechanism is easily understood. Since the U-shaped actuator forms an electrical short loop (current passing through the actuator from cold arm anchor to hot arm anchor), the floating charge can be easily discharged once the POLY0 layer is connected to the cold arm pad (anchor), i.e., type B configuration.

Regarding the pattern design of type B device, because the polysilicon layer is a conducting material, we cannot anchor two pads together onto the same Poly0 layer. Otherwise, the loop from anchor-to-anchor will become open and Joule heating cannot be generated. Furthermore, we have to emphasize here that the Poly0 layer cannot be connected to the hot arm pad, i.e., type C1 configuration because this actuator type will suffer from a more serious electrostatic pulling force. This is because the cold arm has a much larger beam area than the hot arm. In other words, its parallel capacitance effect is stronger. Figure 7 shows the displacement of the tip end of the type C actuator with different "charge" arrangement in each dynamic swing motion, i.e., type C1 and type C2 configurations. Clearly, due to the increased attraction force caused by the electrostatic force at high voltage, the displacement of the type C1 sample became saturated when the applied voltage was higher than 4 V. On the contrary, continuously increasing displacement data were observed in type C2 sample. Moreover, we did not observe any sticking behavior during the actuation in type C2 devices and this is the most important characteristic required for practical applications. Basically, as mentioned in the second part, the type C2 actuator is almost the same as the type B one except that the Poly0 in type B is connected to the cold arm pad directly and not through the probe or the bonding wire. Since the extra wire bonding is not necessary for type B devices, this pattern design will be more convenient and suitable for practical use. These aforementioned results indicate that the design of type B is very helpful for the enhancement of motion stability for the U-shaped electrothermal actuator. This valuable concept can also benefit other electrostatic type actuators which also suffer from electrostatic-induced stiction problems.

Table I. Standard actuator dimensions and definitions for the testing; the results are shown in Figs. 8, 9, 10 and Table II.

Standard testing actuator dimensions	
CW=20 μm; FL=40 μm; HL=250 μm	
Definitions:	CW: Cold arm width
	FL: Flexural beam length
	HL: Hot arm length

3.2 Electrostatic effect and optimum actuator dimensions

Based on the results discussed above, the electrostatic force is seen to have a very significant influence on electrothermal actuator motion. This motivated us to investigate the relationship between the electrostatic effect and the actuators with different dimensions so that a suitable set of dimensions, which could reduce the electrostatic effect, might be determined.

In this section we discuss the standard actuator dimensions and some parameters are listed in Table I. The deflection results shown in Fig. 8 were due to the motion that was not affected by electrostatic force, i.e., of type B devices. We used these data as our comparison references for the electrostatic effect. These test results reveal that the deflection of actuator would increase with cold arm width (*CW*). This is because the current density decreases with *CW* and the Joule heating effect will also be decreased. Moreover, since higher *CW* can also enhance the ability of heat convection, all these effects will result in a larger temperature difference between the hot and cold arms. It can explain why, in the case of $CW > 10\,\mu m$, the deflection would again have a minor increase at high voltage even if it was insensitive to *CW* at low voltage. Regarding flexural beam length (*FL*) and hot arm length (*HL*) parameters, we found that they have an opposite influence on the actuator's deflection. As mentioned above, the motion of actuator mainly consists of driving by the expansion of *HL*. Therefore, there is no doubt that the deflection will increase with *HL*. On the contrary, since the expansion of *FL* would counter the expansion of *HL*, larger *FL* will lead to a decline of deflection. As a result, if the *FL* or *HL* reach the limits of their dimension, i.e., *FL* of 140 and *HL* of 100, a very small deflection would be observed in actuators with these dimensions, as shown in Figs. 8(b) and 8(c). Nevertheless, a very small *FL* ($FL < 20\,\mu m$) and a very long *HL* ($HL > 250\,\mu m$) will also cause the actuator to have difficulty in moving due to the increased stiffness and sagging problem (after the sacrificial layer is released). The analyses above show that, for the actuator's deflection, *FL* and *HL* are more dominating dimension parameters than the *CW* parameter. However, since the *CW* will act as a large parallel capacitance if the actuator is suffering from electrostatic force during the operation, it might become the most dominating dimension parameter for this kind of motion.

We summarize the results of electrostatic effect on the deflection behavior of actuators using different dimensional parameters in Fig. 9. The "manipulated" electrostatic effect

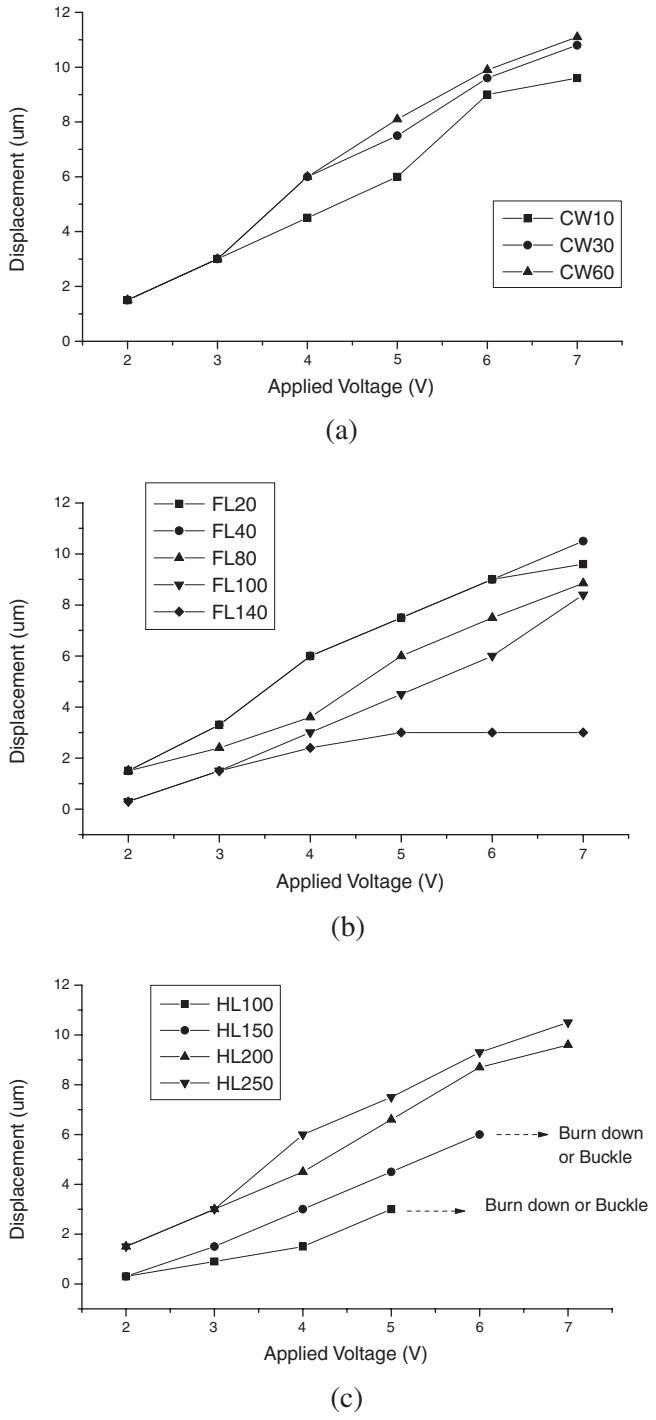

Fig. 8. Measured tip displacement for type B device with different dimensions (a) cold arm width results (b) flexural beam length results (c) hot arm length results.

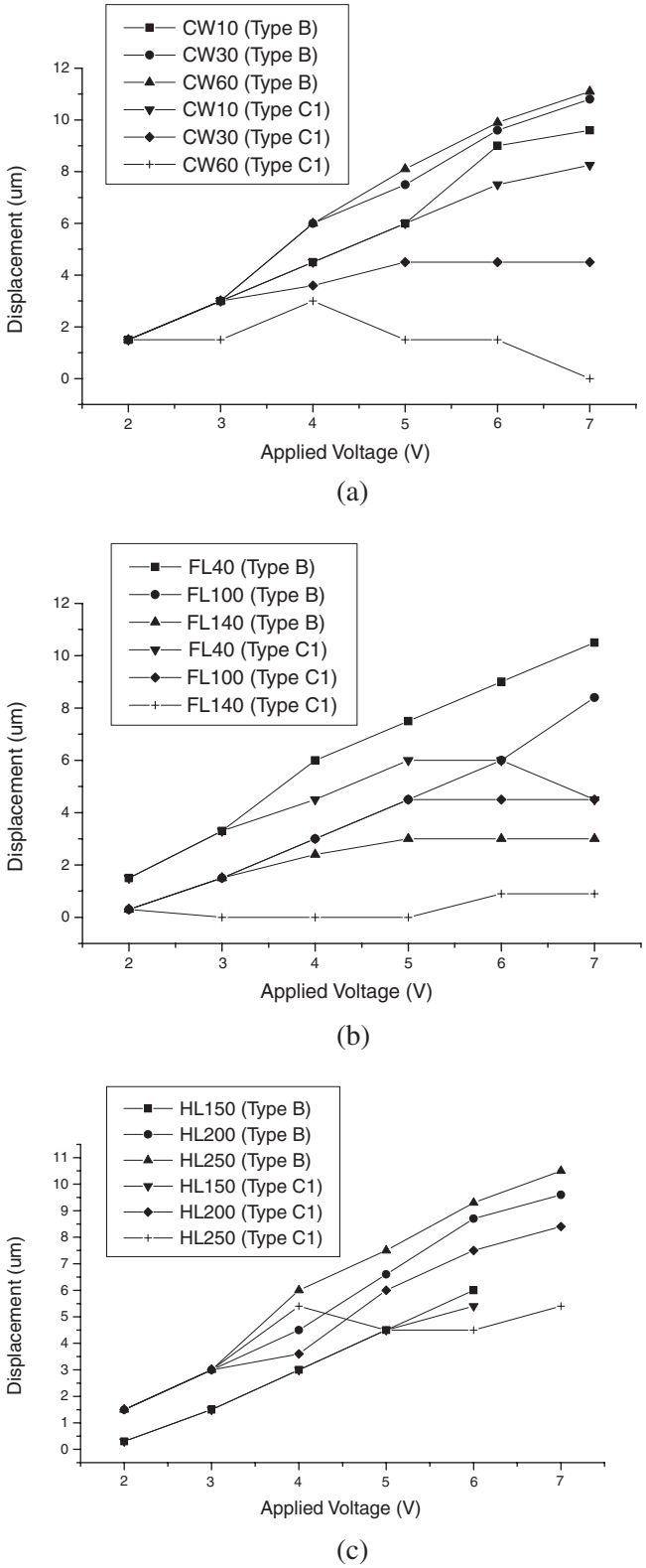

Fig. 9. Measured tip displacement for type B and type C1 devices with different dimensions (a) cold arm width results (b) flexural beam length results (c) hot arm length results.

was created by using the pattern of type C1 device shown in Fig. 2. Since the results in Fig. 9 were attributed not only to the electrostatic effect but also to the mechanical properties of actuators, we have to realize the influence of dimension variation on mechanical properties so that the pure electrostatic effect can be identified. The output force and "anti-sag" stiffness are the most important properties in this problem. Table II and Fig. 10 show the influence of different dimensions on these two properties. They were calculated by FEM simulation and mechanics material theories.

For the CW case, the stiffness is insensitive to the variation of dimensions. The CW30 device can deliver the largest output force. CW60 and CW10 devices exhibit almost the same performance. As discussed above, the CW60 device could exhibit longer displacement if the motion was not interfered with by the electrostatic effect (CW60 > CW30 > CW10). However, results in Fig. 9(a)

Table II. Actuator's stiffness for overcoming electrostatic pulling force (downward).

Actuator's "anti-sag" stiffness (μN/μm)					
CW10	0.161	**FL10**	0.314	**HL100**	1.735
CW20	0.174	**FL20**	0.237	**HL150**	0.629
CW30	0.179	**FL30**	0.198	**HL200**	0.305
CW40	0.180	**FL40**	0.174	**HL250**	0.174
CW50	0.180	**FL60**	0.146	**HL300**	0.110
CW60	0.180	**FL80**	0.129	**HL350**	0.075
CW70	0.178	**FL100**	0.118		
CW80	0.176	**FL140**	0.104		

show that, with the electrostatic effect, the CW10 device became the device with the best displacement performance, instead of the CW60 device (CW10 > CW30 > CW60). Clearly, the electrostatic effect became more dominating for higher CW devices. Since the electrostatic force is highly related to CW, i.e., cold arm area, in order to reduce the electrostatic effect, the CW should be as small as possible. The suggested dimension is less than 10 μm. However, it has to be noted here that the temperature difference between the cold arm and hot arm will also become smaller once the *CW* reduces. It will result in a reduction of deflection. In terms of *FL*, we found that the longer the FL, the smaller are the stiffness and output force and the electrostatic effect will also become weaker with *FL* owing to the reduction of cold arm area. This can explain why, as presented in Fig. 9(b), FL40 device motion was influenced by the electrostatic force at 3 V. However, this critical point was postponed until 5 V for the FL100 device. Furthermore, unlike the FL40 device, the FL100 device did not undergo an abrupt decrease in displacement at a higher voltage (7 V) even when both its output force and stiffness were smaller than those of the FL40 device. Nevertheless, the actuator with a very long *FL* would become very fragile for the electrostatic force because both its output force and its stiffness would be too small. Figure 9(b) supports this analysis. The FL140 actuator would still tend to adhere to the substrate due to the electrostatic pulling force even if the applied voltage was very low (<3 V). As a result, the proper *FL* dimension for reducing the electrostatic effect on the actuator motion should be around 100 μm. Regarding the HL parameter, it plays a positive effect on the output force and a negative effect on the stiffness. However, the electrostatic force will increase with HL due to the larger cold arm area. Therefore, although *HL* can boost the output force, devices with higher *HL* will deflect less due to higher electrostatic force and smaller stiffness. The data depicted in Fig. 9(c) shows that compared with HL150 and HL200 devices, HL250 devices would diminish dramatically. Furthermore, the electrostatic effect starts to affect the motion behavior at 3 V for the HL250 device. On the contrary, this critical point would start later at 5 V for HL150 devices. As a result, the electrostatic effect cannot be minimized until *HL* becomes smaller than 200 μm according to the results in Fig. 9(c).

Based on the discussions above, in order to reduce the electrostatic effect, the suitable dimensions required are as follows: cold arm width = 10 μm; flexural beam length = 100 μm; and hot arm length = 200 μm. However, this treatment has to be at the expense of the actuator's performance: such as lower output force and smaller displacement. This will not be acceptable for practical applications. This result indicates that the design of type B will be required for these kinds of device applications. Since we can easily eliminate the influence of electrostatic force on the actuator motion by using the design of type B device, we can decide the optimized dimensions for the actuator based on the results in Fig. 8. After a thorough analysis, we

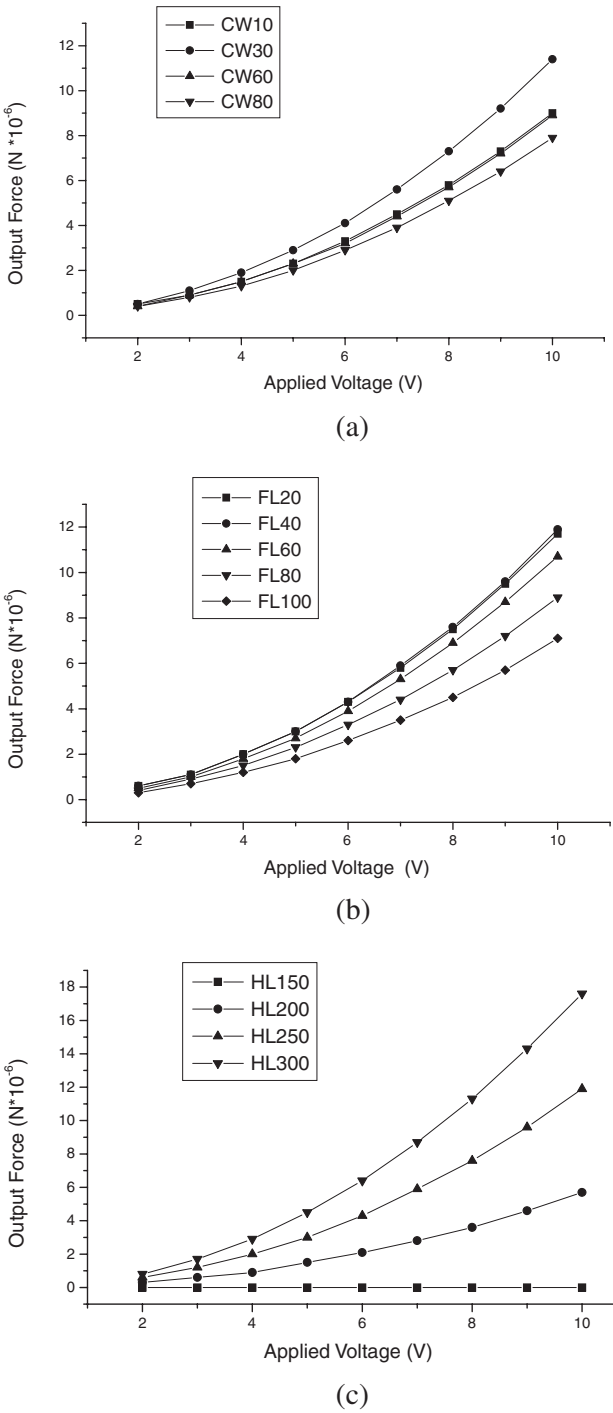

Fig. 10. Calculated output force of actuators with different dimensions (a) cold arm width results (b) flexural beam length results (c) hot arm length results.

suggest that the ideal dimensions for the device that can exhibit larger deflection, and higher output force may be $CW = 30\,\mu m$; $FL = 40\,\mu m$, and $HL = 250\,\mu m$.

4. Conclusion

We have determined the reasons why the U-shaped thermal actuators often stick and adhere onto their underlying layers during operations. The origin of these motion instabilities is mainly attributed to electrostatic force due to the floating charge accumulation. It is concluded that the proper design of such actuators should include an underlying polysilicon layer in order to achieve a stable motion behavior. The suitable dimensions for reducing the electrostatic effect on the actuator's motion are presented. However, since these dimensions will result in poor displacement and output force performance, they are not recommended for use in practical applications. By using the proposed polysilicon layer pattern design, the optimized dimensions for the actuator have been finally decided as follows: cold arm width $= 30\,\mu m$; flexural beam length $= 40\,\mu m$ and hot arm length $= 250\,\mu m$. Based on these suggested dimensions, the actuator can exhibit $10\,\mu m$ displacement and around $6\,\mu N$ output force at an applied voltage of 7 V.

1) J. H. Comtois and V. M. Bright: J. Sens. & Actuat. A **58** (1997) 19.
2) C. S. Pan and W. Hsu: J. Micromech. Microeng. **7** (1997) 7.
3) E. S. Kolesar, S. Y. Ko, J. T. Howard, P. B. Allen, J. M. Wilken, N. C. Boydston, M. D. Ruff and R. J. Wilks: J. Thin Solid Films **377–378** (2000) 719.
4) D. A. Koester, R. Mahadevan, B. Hardy and K. W. Markus: *MUMPs Design Handbook* (Cronos Integrated Microsystems, NC, 2001) Rev. 7.0.